Robotics and Autonomous Systems 74 (2015) 351–359

Contents lists available at ScienceDirect

Robotics and Autonomous Systems

journal homepage: www.elsevier.com/locate/robot

A thermographic visual inspection system for crack detection in metal parts exploiting a robotic workcell

Stefano Ghidoni *, Mauro Antonello, Loris Nanni, Emanuele Menegatti

Department of Information Engineering, University of Padova, via Ognissanti, 72 — I-35129 Padova, Italy

HIGHLIGHTS

- Thermography was explored as a means for the detection of micro defects.
- We developed a system capable of finding cracks in metal parts using thermography.
- The system is very robust thanks to the complete knowledge of the imaging process.
- The system is able to deal with parts of very complex geometry.
- The proposed inspection method is cleaner than other alternatives currently in use, and does not use polluting substances.

ARTICLE INFO

Article history:
Available online 9 September 2015

Keywords:
Computer vision
Automated visual inspection
Thermographic image analysis
Knowledge-based image analysis
Pattern recognition

ABSTRACT

Cracks are the main source of failure in the production of metal parts: systems for checking their presence are therefore crucial for defect-free production. In this paper, an autonomous system for performing this quality control is presented. The system is equipped with a heating tool, a thermocamera, and a robot to handle the part. The inspection process is based on the observation of the propagation of thermal waves through the inspected part, a method that can highlight very small cracks with high reliability. A knowledge-based approach to visual inspection is exploited for detecting the cracks: all the system parameters are known by means of an accurate calibration of the workcell. The system was tested on a large dataset and demonstrated its capability of detecting tiny production defects, that can lead to dangerous failures when the metal components are put under strong mechanical stress.

1. Introduction

Visual inspection is the key to defect-free manufacturing. A vision system that checks the parts along the production line offers multiple advantages, first of all the capability of analyzing each produced piece, that is a crucial requirement to satisfy the highest quality standards. Systems employed for visual inspection need to adapt to the parts to be checked: the complexity of such systems therefore ranges from light units, running on rather simple embedded hardware, to complex combinations of cameras, lighting, and robotics [1–3].

Focusing on the production of metal parts for high-performance components, like crankshafts for combustion engines, one of the main source of failure is represented by the presence of cracks: even very small fractures of the metal structure can break the part when it is subject to strong mechanical stress. Currently, the presence of cracks is performed using Magnetic Particle Inspection (MPI): the part to be analyzed is first washed, then put into a magnetic field and finally covered with magnetic particles, either in the form of a dry powder, or, more frequently, in a wet suspension. Cracks are detected because they cause leaks in the magnetic flux; such leaks are highlighted by the particles, which can be inspected by means of a UV light. The whole process is very complex and needs to be done manually; it is also extremely time-consuming, because parts need to be cleaned, magnetized, covered with magnetic particles, inspected, de-magnetized and cleaned again. Moreover, magnetic particles and their carrier are a source of pollution, and should be properly processed after use, with high costs.

Even though MPI is still used in industry, current technology offers a large set of tools that enables the introduction of alternative inspection methods, that offer the advantage of being green, fast, and automatic. Investigating how it is possible to replace MPI with more modern technology was the goal of the ThermoBot project

* Corresponding author. Tel.: +39 334 6575827.
E-mail addresses: ghidoni@dei.unipd.it (S. Ghidoni), mauro.antonello@dei.unipd.it (M. Antonello), nanni@dei.unipd.it (L. Nanni), emg@dei.unipd.it (E. Menegatti).

http://dx.doi.org/10.1016/j.robot.2015.07.020
0921-8890/

(www.thermobot.eu) funded by the European Commission in the Factory of the Future research program. A major advantage of visual inspection systems is that they are able to analyze parts exploiting not only cameras working in the visible domain, but also in different ones, like near infrared [4], far infrared [5,6] and X-rays [7]. This opportunity is exploited in the project, as its driving idea is to exploit thermography to replace MPI. The project goes beyond crack detection in metal parts: analysis of non-metallic materials, like carbon fiber, are also faced.

The two inspection systems developed in the project share the feature that inspection is performed by means a thermal excitation method (e.g. a laser or a high-power lamp) and a far infrared (FIR) camera, that observes how the heat diffuses inside the part: since defects cause alterations on the heat flux, such alterations can be exploited to inspect the part. This enables the system to detect not only cracks in metal parts, but also inspect inner defects in CFRP (Carbon Fiber Reinforced Plastic) parts.

This paper describes the system developed for detecting cracks in metal parts [8,9]. The paper is structured as follows: in Section 2 the state of the art is revised, while the system structure is explained in Section 3. The core of the visual inspection system, including the knowledge-based approach, that enables the inspection of very small defects, is detailed in Section 4, and the results obtained during the experiments are described in Section 5. Section 6 reports the final remarks.

2. State of the art

The topic of crack detection has been tackled in a number of different ways in the literature, given the strong importance of this type of quality check. A variety of approaches have been used, like the propagation of ultrasounds that is used in [10] to detect cracks and lamination defects in metallic pipes, or Eddy currents [11–13]. Other methods exploit magnetic cameras to detect cracks in parts that are at high temperature [14], or magnetic flux leakage [15], while the method described in [16] studies the heat produced by the Joule effect.

Methods based on image analysis have also been exploited in the literature, ranging from detection of welding defects in pipelines [17] to concrete surface analysis [18] and the protection of cultural heritage [19]. Thermographic image analysis systems have recently been proposed for performing in-situ non-destructive inspections during thermomechanical fatigue tests [20]; the system showed a high sensitivity, being able to detect cracks smaller than 500 μm. The system proposed in [21] is slightly different from the others discussed above as it is meant to inspect different types of materials during fatigue tests, and detect the cracks as soon as they appear.

Thermography-based crack detection is often coupled with excitation methods like eddy currents [22] or laser beams; in particular, lasers provide the inspection process with high flexibility, as it is possible to concentrate the heat on a small spot, and enabling and disabling the heat source can be done instantly, generating pulses at high frequency. This last characteristic is exploited in pulse thermography and techniques that are derived from it [23]. Another technique based on laser technology is the "flying spot active thermography" [24], that refers to a laser spot that causes a local excitation on the part under inspection. This is similar to the analysis method employed in the ThermoBot project, and was chosen in [24] to inspect high pressure turbine blades.

3. A visual inspection system for crack detection

The inspection process described in this paper is based on the analysis of how thermal waves propagate through a metal part.

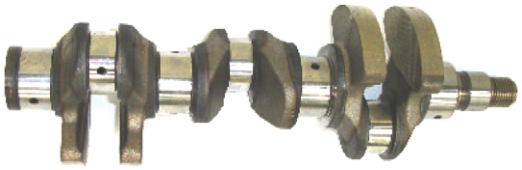

Fig. 1. The sample part used for the experiments: a metal crankshaft.

The inspection cell is composed by a laser, a thermocamera, and a robot. The laser is exploited to generate the thermal excitation and the robot is used to move the part, in order heat and inspect different regions of the part. The thermal waves are acquired by the thermocamera and automatically processed. To obtain highly detailed images and enhance the sensitivity of the system, the FOV (Field Of View) of the camera is narrow, therefore only a small region of the inspected part can be viewed. This does not limit the system, because only a small area around the laser spot is affected by the thermal waves.

The introduction of the robot in the inspection cell is needed because the thermal waves are generated by moving the heat source over the part. Moreover, the capability of moving the sample is crucial for inspecting parts of complex shape that causes a large number of self-occlusions, i.e. some sections of the inspected part hide other sections, depending on the perspective under which the item is framed. The robot is able to change such perspective, letting the system analyze the whole surface. Thanks to the robot, the visual inspection system offers a high level of flexibility, that enables it to inspect parts of very different size and shape.

3.1. Test samples

The system described above is meant for analyzing metal parts, that require a powerful heat source. The sample parts exploited in the experiments are heavy metal crankshafts, shown in Fig. 1.

To perform the analysis, the part is first fixed to the robot, whose movements determine which regions are thermally excited by the laser and framed by the camera. The robot path is automatically generated, based on the part geometry (provided as CAD data). The inspection process requires the laser to go over every area that should be checked: this leads to a long processing time for parts that are rather large, and have a complex geometry, as for the crankshaft of Fig. 1. To reduce the time needed, a set of regions where cracks are more critical was defined, and the analysis is restricted to those areas only.

3.2. Inspection system workcell

The scheme of the inspection system workcell is shown in Fig. 2(a). In (b) it is possible to see the components of the workcell: the yellow robot is clearly visible, the laser is the metal box on the top, while the thermocamera is the red box on the top right corner. During the inspection process, the robot places the part in a zone in which the camera FOV and the laser beam intersect: the crankshaft in Fig. 2(b) is in that area.

As said above, the workcell hosts a powerful laser source: when it comes to heavy metal parts, the amount of energy needed for generating a heat wave that is visible with a thermocamera is rather high: a source reaching a power level of 7 W was chosen in our case. The speed at which the laser spot runs over the inspected part (called "laser speed") is an important system parameter.

The robot path planning is performed in order to guarantee a laser speed which is almost constant, that should be related with the time needed for the heat to diffuse through the metal. For example, a low laser speed leads to a diffused heat that would make

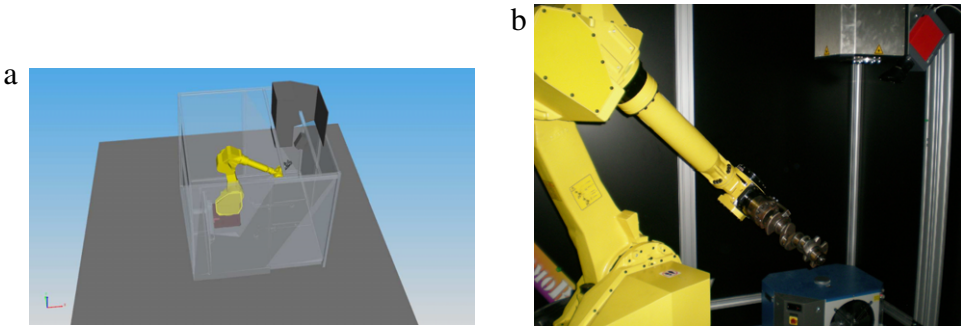

Fig. 2. Scheme (a) and picture (b) of the workcell for inspecting metal parts. (For interpretation of the references to color in this figure legend, the reader is referred to the web version of this article.)

it impossible to detect cracks. On the other hand, a very high speed strongly reduces the energy going into the part, and leads to weak thermal waves. The best choice for this parameter, which is the value we used for the experiments, is 100 mm/s.

3.3. Knowledge-based inspection process

The main feature of the inspection system is the high level of knowledge of all the elements that influence the scene framed by the camera and the image formation. There are three types of information that are needed. The first is about the physical structure of the system, that includes the knowledge of the camera parameters and of the reciprocal position and orientation of the three elements building the system. This is recovered by performing a workcell calibration, that is done considering the camera as the reference: both a laser-camera and a robot-camera calibration are run. This calibration needs to be performed only once, and data provided by such process is valid until one of the three elements of the system is moved.

The second type of information needed is given by the CAD model of the inspected part, and the geometry of the gripper used for moving the part. This information needs to be provided for every new part that is inspected by the system. As mentioned above, the CAD data may contain critical areas to which the inspection shall be restricted in order to speed up the process.

The third type of information exploited by the system is the current status of the robot, that is the only element that changes its geometry during the inspection. The software framework controlling the workcell needs to guarantee a very accurate synchronization between robot and camera, in order to associate the correct robot position to each image acquired. This is needed in order to recover the position of the inspected part in a given image, which has an impact on the projection modules that will be described in Section 3.4.

The information mentioned above is the key to the knowledge-based approach exploited for performing image segmentation. This expression is commonly used in the literature to indicate that a priori information is available about the observed phenomenon, e.g. the shape of the object to be detected [25,26]. In the context of the Thermobot project, the inspection is said to be knowledge-based because several modules of the system exploit information about the workcell: this applies, for example, to the image segmentation described in Section 4.1 and to the analysis on thermal persistence, discussed in Section 4.3.

The choice of developing a knowledge-based approach is crucial to enhance the detection performance and to filter out several noise factors that affect the imaging process. The thermal waves generated by the laser source need to be distinguished from other phenomena that generate similar patterns on the image, e.g. reflections caused by the shiny surfaces of the metal parts.

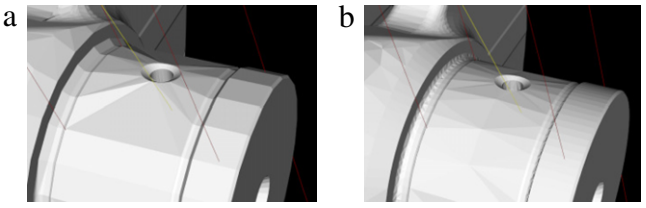

Fig. 3. Different accuracy in mesh generation: a mesh can be generated using a lower number of larger elements (a) or a higher number of smaller elements (b).

3.4. Forward and backward projections

The module that most deeply exploits the available system knowledge is in charge of evaluating forward and backward projections, that is, projecting points from 3D world coordinates to 2D image coordinates, and vice-versa. More specifically:

- given a point on the 3D CAD model of the inspected part, determine in which point of the image it is projected in the current configuration of the acquisition system;
- given a pixel (or a group of pixels), determine which area of the inspected part was projected on such pixels.

The projection module is exploited for evaluating the laser spot center on the image and to measure the thermal persistence described in Section 4.3. This transformation requires an extremely high accuracy for the synchronization between camera and robot. The 3D CAD model is represented in terms of a mesh, that is, a set of triangles and vertices. This representation is a common choice, and can be derived from multiple CAD file formats—the Open Cascade Technology (OCCT)[1] was used in our system. The mesh can be generated using different accuracy levels, that lead to larger or smaller mesh elements, as it can be seen in Fig. 3.

An example of projection is shown in Fig. 4. In the lower half of the image a portion of the CAD model is visible, that corresponds to the region framed by the camera. In the upper half of the image it is possible to see the result of the projection module, that substituted the points on the mesh surface with pixels coming from the input image, and projected onto the CAD model.

In the following, the three elements building the projection module will be detailed.

3.4.1. Laser-mesh projection

This sub-module finds the projection point of the laser onto the piece mesh, in particular it retrieves the point over the first mesh triangle hit by the laser ray. In order to avoid unnecessary computation, a Z-buffering algorithm has been used to sort triangles

[1] http://www.opencascade.org/.

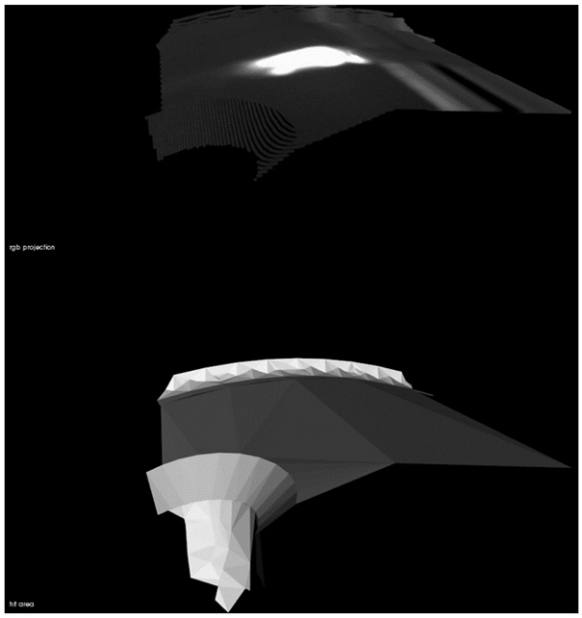

Fig. 4. Example of projection results. In the lower part of the image, the portion of the CAD model corresponding to the region framed by the camera is visible. In the upper part of the image, the same region of the inspected part is obtained by projecting the 2D image pixels onto the CAD model.

with respect to their distance to the laser origin and direction. The ray-triangle intersection test has been implemented following the procedure proposed by Möller et al. [27]. Fig. 5(a) shows the projection point $\mathbf{P}_w$ of the laser ray onto the piece the mesh.

3.4.2. Mesh-camera projection

This component makes use of the camera intrinsic and extrinsic parameters to compute the projection of a 3D point on the camera projection plane (1). Intrinsic parameters are expressed as a camera calibration matrix $\mathbf{K}$ while the extrinsic parameters consist of the camera translation $\mathbf{C}$ and orientation $\mathbf{R}$ with respect to the world origin. Using the homogeneous coordinates convention,[2] the 2D projection point $\mathbf{P}_I$ of the 3D point $\mathbf{P}_w$ is given by:

$$\lambda \mathbf{P}_I = [\mathbf{K}_C | \mathbf{0}_3] \begin{bmatrix} \mathbf{R} & -\mathbf{RC} \\ \mathbf{0}_3^T & 1 \end{bmatrix} \mathbf{P}_w, \tag{1}$$

where λ is the homogeneous scaling factor. Fig. 5(b) shows the projection of the point $\mathbf{P}_w$ to $\mathbf{P}_I$ on the camera image plane.

3.4.3. Camera back-projection

The camera back-projection component finds the ray corresponding to the back-projection of a 2D point on the camera image plane back to the 3D world. Given a 2D point $\mathbf{P}_I = (x, y, 1)^T$ on the image plane, there exists a set of 3D points that are projected to $\mathbf{P}_I$. This set of points is distributed along the ray $\mathbf{P}(\lambda)$ connecting the camera center $\mathbf{C}$ and the 3D point corresponding to $\mathbf{P}_I$, given by:

$$\mathbf{P}(\lambda) = \mathbf{C} + \lambda \mathbf{R}^{-1} \mathbf{K}^{-1} \mathbf{P}_I. \tag{2}$$

Fig. 5(c) shows the back-projection of the point $\mathbf{P}_I$ to a 3D ray $\mathbf{P}(\lambda)$.

4. Image processing for crack detection

The core of the crack detection system is the image processing module, whose task is to analyze the acquired images, in which it is possible to see the heat diffusion. The crack detection algorithm focuses on the heat source, namely the laser spot, and analyzes its shape and deformations. The main blocks of the image processing module are summarized in Fig. 6: the spot contour is extracted, and its shape measured by means of features, that are in turn used to feed a classifier.

4.1. Laser spot segmentation

The first step of the image processing is the segmentation of the laser spot. This task follows the knowledge-based approach, since the center of the spot is provided by the system, as explained in Section 3.3: the system knows the location of the inspected part, and the direction of the laser beam; it is therefore possible to calculate the point in which the beam hits the part. Such 3D point is then projected onto the image exploiting the projection module described in Section 3.4. Knowing the location of the laser spot in the image is particularly helpful when reflections are present in the image, as they show up as saturated areas, similarly to the laser spot.

The laser beam is modeled as a line: the system therefore provides just a point on the image, that represents the spot center. However, the crack detection algorithm is based on the analysis of the contour of the spot: this needs to be segmented analyzing the image. The algorithm for segmenting the image is based on the following steps:

- adaptive thresholding, for isolating the bright area around the given spot center;
- application of morphological operators for reducing noise;
- extraction of the spot contour.

The adaptive thresholding is exploited to binarize the input image depending on the image contrast and brightness, that can change depending on the camera automatic gain level. The morphological operators help to smooth the noise affecting the contour: the binarization often provides a rather irregular shape, that is a strong noise source affecting the evaluation of the feature. The third step mentioned above is the contour extraction, that transforms a group of pixels into the higher-level contour representation.

In Fig. 7 some results of the hotspot extraction algorithm are represented: the spot is correctly segmented when its shape is deformed and the center of the laser beam is far from the center of the hot region (a) and (d). The algorithm provides good results also when the hot spot location is close to the image edge (c), and other spots are in the image, because of a crack (b) and (c).

4.2. Spot shape measurement

The shape of the contour extracted from the hotspot is measured by means of features, as summarized in Fig. 6. Each feature is evaluated around the hotspot contour, that is, in a small crop of the original image, that includes the hot spot. Several features were exploited in this work, in order to gather a high level of detail: the best results were achieved using Radial Density Profile (RDP), Weber's Law Descriptor (WLD), Pyramid Local Binary Pattern (PLBP) and Morphological Features (MF), that are detailed in the following.

4.2.1. Radial density profile

The RDP method [29] is a general-purpose feature for measuring texture. Since pixels composing the texture are considered along circular patterns, this method is effective when patterns to be considered have a circular or quasi-circular shape. The RDP was used to characterize medical images containing viruses: such medical images are rather similar to the case of laser spot analysis as in both cases it is important to study the circular shape of an object.

The RDP is exploited to analyze the area around the laser spot and possible deformations of the heat flow, or of the laser spot itself. The RDP is evaluated on the area around the laser spot: a

[2] For an exhaustive introduction to the computer vision concepts used here, please refer to [28].

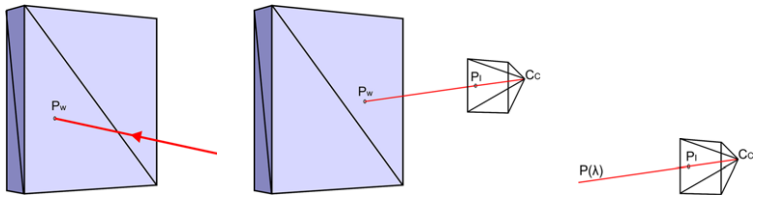

(a) Laser-mesh. (b) Point-image. (c) Backprojection.

Fig. 5. Working principle of the projection module: projection point $\mathbf{P}_w$ of the laser onto the piece mesh (a), projection of the point $\mathbf{P}_w$ to $\mathbf{P}_I$ on the camera image plane (b), and back-projection of the point $\mathbf{P}_I$ to a 3D ray $\mathbf{P}(\lambda)$ (c).

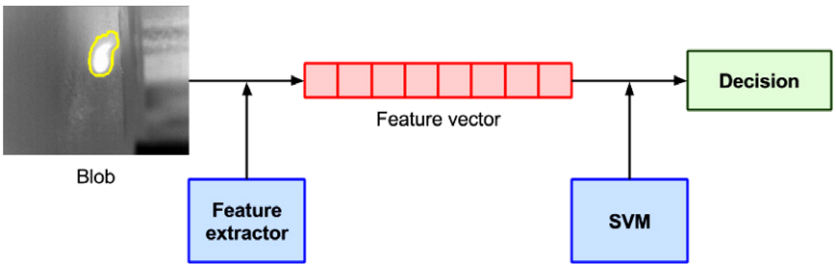

Fig. 6. Scheme of the image processing system for crack detection. The laser spot is segmented in the image, and its shape is measured by means of features, which are in turn used to feed a classifier.

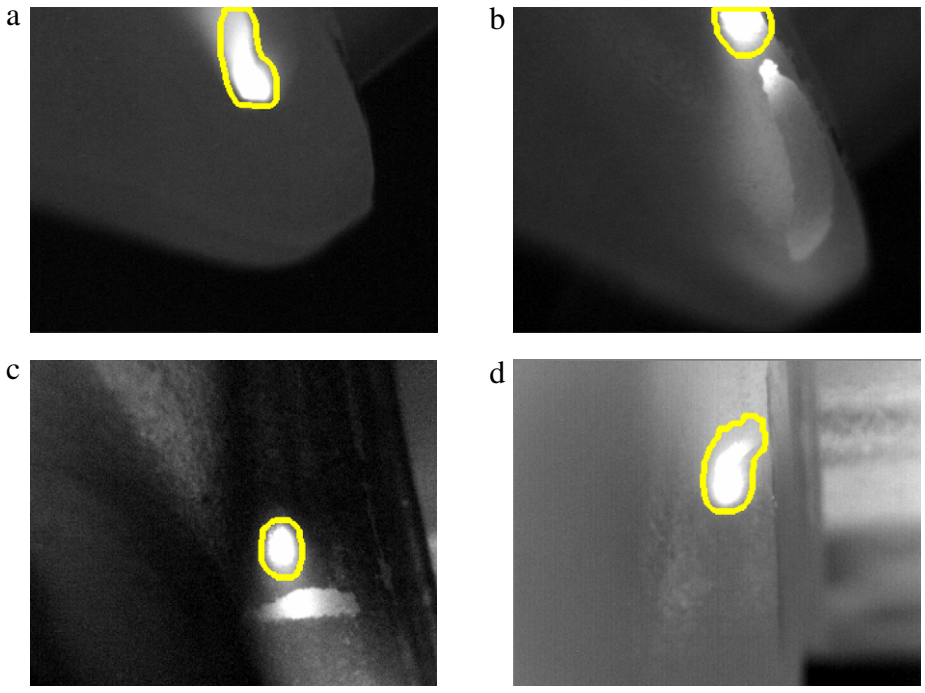

Fig. 7. Examples of hot spot extraction: in (a) the laser spot deformation is caused by the hot region corresponding to the previously heated positions. In (b), a crack prevents the heat to uniformly diffuse through the metal; this appears as two hot spots that are jointly segmented. In (c), the real hot spot is correctly distinguished from the one generated by the crack. Finally in (d) is shown an example of correct separation between the real laser spots and other hot regions caused by cracks.

crucial part of this method is the reliable extraction of the spot itself, and of the surrounding area. In principle, identifying the laser spot is an easy task, because it is the lightest part of the image. However, several noise factors might arise, like reflections on shiny parts, and deformations caused by previous positions of the laser spot, that still have a high temperature. Substantial work was devoted to increase both reliability (i.e., the correct hot spot is filtered from reflections and other hot areas) and accuracy (i.e., the right shape is extracted) of this low-level algorithm.

4.2.2. Weber's law descriptor

Weber's law descriptor (WLD) [30], is a descriptor based on Weber's law. Developed in the field of experimental psychology, it describes the relationship between the increment threshold ΔI, i.e. the minimum noticeable difference in a stimulus intensity that can be detected by a human being, and the initial stimulus intensity I. The relationship states that:

$$\frac{\Delta I}{I} = k, \tag{3}$$

where k is a constant. If the change is less than this constant ratio then it is considered background noise. The ratio $\Delta I/I$ is also known as the Weber's fraction. In other words, the Weber's law states that when a human being is subject to a given stimulus, the lower the level of such stimulus, the smaller the variation he can notice. In the evaluation of WLD, the concept of salient variation

is applied to the difference in gray level between neighboring pixels.

4.2.3. Pyramid local binary pattern

Pyramid Local binary pattern (PLBP) [31] is a variant of Local Binary Pattern (LBP) [32] based on the Gaussian Pyramid Decomposition of the original image. Standard LBP labels each pixel x of a given image with a binary label based on the comparison of the intensity of the pixel itself and P surrounding pixels located at distance R from x. Differently, in PLBP each level $l = (0, \ldots, Lev)$ of the Gaussian pyramid is built by blurring and downsampling the previously computed level; LBP is then applied to each of the Lev levels. We considered $Lev = 2$ including level 0, i.e. the original image. Blurring and downsampling were performed respectively by applying a 5×5 lowpass kernel and a downsampling ratio $R_x = R_y = 2$. The chosen LBP operator is the uniform bins with $(P = 8, R = 1)$ and $(P = 16, R = 2)$.

4.2.4. Morphological features

Morphological features (MF) is a technique originally developed for analyzing Indirect Immunofluorescence (IIF) images, a technique used in medical imaging for analyzing cells and tissues [33]. Using the maximum and the minimum intensity values of the image, a set of 20 equally spaced thresholds is evaluated: each one is then used for generating a binary image. For each of the binary images 6 features are extracted: (i) number of objects, (ii) total area, (iii) area of the convex hull, (iv) eccentricity, (v) Euler number and (vi) perimeter. Each binary image is also used to create 20 cut-outs from the original image for extracting features based on intensity and entropy.

The procedure described above is applied three times: the first time to the acquired image, the second and third times to the smoothed copies of the original image, using two different Gaussian kernels. The final feature vector is obtained by combining the features obtained this way; such combination leads to a rather large feature vector, containing 966 elements.

4.3. Analysis of thermal persistence

In addition to the hotspot analysis described in Section 4.2, a further inspection method was developed, that is called ATP (Analysis of Thermal Persistence). This method is based on the observation that a crack prevents or at least limits the heat diffusion through the part, which possibly causes some energy to accumulate in some regions. This gives rise to a sort of secondary hotspot, as it is the case of Fig. 7(b). The ATP is capable of detecting this effect, that is always connected with the presence of a crack.

Analyzing the available dataset it was observed that a crack does not always cause a heat accumulation: this happens in half of the cracks. This means that this method alone cannot be the core of a crack detection system; however, the detection of heat accumulation is an important complementary module to the spot shape analysis, because it can observe an effect that happens at a distance from the main hotspot, and which is therefore not possible to detect by looking at the laser spot neighborhood.

The ATP works by recording the 3D coordinate of the point in which the laser beam hits the inspected part, exploiting the projection module described in Section 3.4. Such coordinate is saved for each image, which means that the laser trajectory on the part is sampled at the camera acquisition frequency, namely 80 Hz, which ensures a very accurate description. The locations on which the laser hits the part in the past are obviously constant in 3D world coordinates. However, they change from frame to frame in the 2D image domain, because the perspective from which the camera frames the part changes continuously, driven by the robot motion. Since the ATP needs to analyze the image in those regions that were heated in the past, the hit locations in 3D need to be projected onto the 2D image domain at each new frame that is processed.

Once the locations of the previously heated positions are available in the current image, the ATP checks the thermal status of the regions corresponding to such positions; regions are defined considering a circular shape around each heated position and sampling some points inside such circle. Points selected this way are analyzed by considering the gray level of the thermal image: such level is considered together with time instant in which that region was heated. Regions that show a high energy level after a long time reveal the presence of a crack.

5. Experimental results

The system described so far was tested using the crankshafts described in Section 3.1, that are produced by BRP Powertrain, one of the partners of the Thermobot project. As it can be seen from Fig. 1, the geometry is extremely complex, and fully exploits the flexibility provided by the articulated robot. Cracks affecting the sample parts are extremely small: the length is in the order of 1–2 mm, while the thickness is in the order of 50 μm.

5.1. Types of surface of the metal parts

In Fig. 1, it is possible to see that the part shows two different types of surfaces, that are either rugged or polished. While in the former case it is rather easy to heat the part and perform the inspection, the latter surface is extremely difficult to analyze, because almost all the energy of the laser beam is reflected. The way surfaces are finished is the main aspect influencing the visual inspection process; other factors, for example the non-uniform metallographic structure due to the forging process, do not cause any visible influence on the heat transfer.

The analysis of polished area turned out to be unfeasible using the laser as a heat source, even by applying a graphite coating on the part: the resulting images are like the one shown in Fig. 8. Looking at the image it is possible to see that the laser spot, in the red box, is very hard to see, while reflections (in the green boxes) create stronger patterns. Even though the projection module described in Section 3.4 provides information about the right location of the spot, the spot in the red box is nevertheless too weak to be effectively analyzed using the techniques reported in Section 4.2; the ATP is also ineffective: there is no persistence, since even the main spot is not clearly visible.

Even though alternative heating methods exist, e.g. induction heating, the laser beam is the only method that can be applied to parts of complex shape: for example, induction works effectively only if the inductor (the element used for inducing currents in the part to be heated) has a shape similar to the part to be inspected. This means that a different inductor would be necessary for each type of curvature to be analyzed. The laser was therefore chosen because it is the only way to analyze parts of any shape, even though not all surfaces can be inspected.

5.2. Laser spot classification

The features described in Section 4.2 are used as input to a classifier, that was chosen to be a Support Vector Machine (SVM) [34]. SVMs are general purpose binary classifiers which learn the boundary between samples of two different populations, projecting the samples into a multidimensional feature space and drawing a separating hyperplane. An SVM is a maximum margin classifier: it finds a decision surface that maximizes the distance of the closest points in the training set to the decision boundary. Several kernel functions (e.g. linear, polynomial, and radial basis functions) can be used as approximating functions.

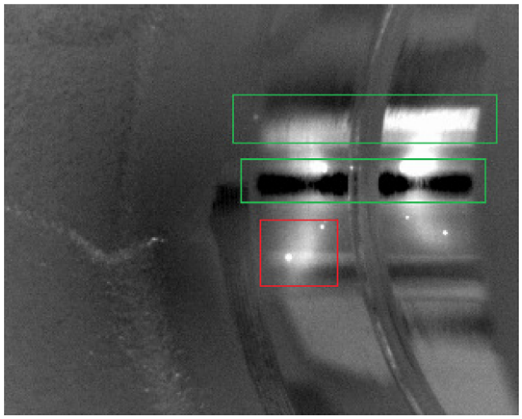

Fig. 8. Image acquired when the laser hits a polished part of the crankshaft. The pattern generated by the laser beam (red box) is very weak, and it is not suitable for being analyzed. The green boxes highlight the reflections. (For interpretation of the references to color in this figure legend, the reader is referred to the web version of this article.)

In this study, radial basis function kernel was employed, as it better adapts to the characteristics of the available dataset, which is composed by a large number of images that were extracted by a reduced number of sample parts. Usually, hundreds or even thousands of samples are used to train a classifier, but this was not possible in our case, since parts that can be used for training are crankshafts with production defects, that are not very common. No parameter optimization was performed, in order to avoid overfitting. The parameter setting exploited for the experiments is rather common: $\gamma = 0.1$; $cost = 1000$.

An important characteristic of the SVM is that it requires a fixed number of input data. This means that the length of the feature vectors used as input to the SVM needs to be constant. However, the feature length depends on the size of the hot spot, and is generally different for each input image that is analyzed. To cope with this issue, it is necessary to resize every blob found in the image to a fixed-length window prior to evaluate the features described above. The size of such window was chosen to be close to the typical dimension of a hot spot, in order to limit the loss of detail caused by the resize operation.

The dataset used for the tests is made of the acquisitions of 9 different parts, for a total of more than 6000 frames. All the parts used in the experiments show a crack in the rugged part, for what was previously said. Since the dataset contains data from 9 different sequences, the "leave-one-out-sequence" testing protocol was adopted, with a 9-fold cross validation: in each fold the data from 8 sequences are used to train the SVM, and the patterns of the remaining sequence are used for testing the system. This procedure is performed 9 times, in this way each pattern is used once as test pattern.

The area under the ROC curve (AUC) [35] is exploited as a performance indicator, and is reported for all the features used in the system. The AUC can be interpreted as the probability that SVM will assign a higher score to a randomly picked positive pattern than to a randomly picked negative one. The AUC evaluated for the approaches employed in the system are reported in Table 1: besides the different approaches discussed, the best-performing combinations of more than one approach are also mentioned. The combination is performed employing the sum rule.

The reported detection performance is frame-based, i.e. every frame was separately classified and compared with the ground truth. This makes it possible to understand the detection capability of each method. However, the inspection system needs to provide a feedback on the whole part, not on the single frames. Therefore, the results on the single frames are combined to provide a per-part classification, rather than a per-frame outcome. It was experimentally observed that the best choice in this case is to declare that a part includes a crack if it is found in two consecutive frames: this is enough to reject the spurious false positives.

Table 1
AUC of the crack detection algorithm using the different features employed by the system. Such features are RDP (Radial Density Profile), WLP (Weber's Law Descriptor), PLBP (Pyramid Local Binary Pattern), and MF (Morphological Features). The '+' sign indicates fusion of two or more methods, combined by sum rule.

RDP	WLP	PLBP	MF	PLBP + MF	WLP + PLBP + MF
68.8	73.9	77.08	77.47	81.47	83.30

5.3. Thermal persistence

The ATP was tested independently from the laser spot classification, because the two systems run in parallel. During the tests, the ATP showed very strong performance, since it provided no false positives nor false negatives. Unfortunately, the thermal persistence can be observed only in 56% of the sequence acquired. In Fig. 9 it is possible to see the result of this kind of analysis: in (a) is represented the normal working condition when no thermal persistence is detected; the points corresponding to the previously heated regions are drawn in the image—the darker the color, the colder the region. In (b) the reaction of the algorithm when some thermal persistence is found is shown: some of the sampled points become lighter. The image in (c) represents the same scene once the thermal persistence faded out: the algorithm nevertheless tracks the persistence that was observed, which is indicated by the red dots (now superimposed to a rather cold region). In (d) it can be seen that the ATP works also when the thermal persistence is joint to the laser blob.

The decision rule for merging the laser spot classification and the ATP into an overall classification result is an or-condition: the part is considered to include a crack if at least one of the two systems finds it. This reflects the fact that the two systems look at two different effects, each one being capable of detecting a crack.

6. Conclusions

In this paper a system for automatic crack detection in metal parts was described. The system is based on a workcell composed of a robot, a thermocamera and a laser source: such elements are able to create thermal waves traveling through the inspected parts and to observe their propagation. The system is equipped with a computer vision software module that is able to automatically detect the thermal waves and detect cracks by observing the deformation of the laser spot and the persistence of thermal energy in the part.

The strong point of the system is the high level of knowledge of the imaging system, which is exploited to drive the computer vision algorithms that perform the low- and mid-level image processing. The introduction of high-level information to help image segmentation is crucial to provide good performance in the considered scenario: heat sources used when acquiring thermographic images of metal parts typically generate a huge number of reflections and artifacts, that could lead to a large number of wrong detections and classifications.

Several tests were run employing very complex test parts, namely crankshafts, showing extremely small cracks. Experiments assessed the very good performance of the system, achieved thanks to the knowledge-based approach presented in the paper.

Acknowledgment

The research leading to these results has received funding from the European Union, Seventh Framework Programme (FP7/2007–2013), under grant agreement No. 284607.

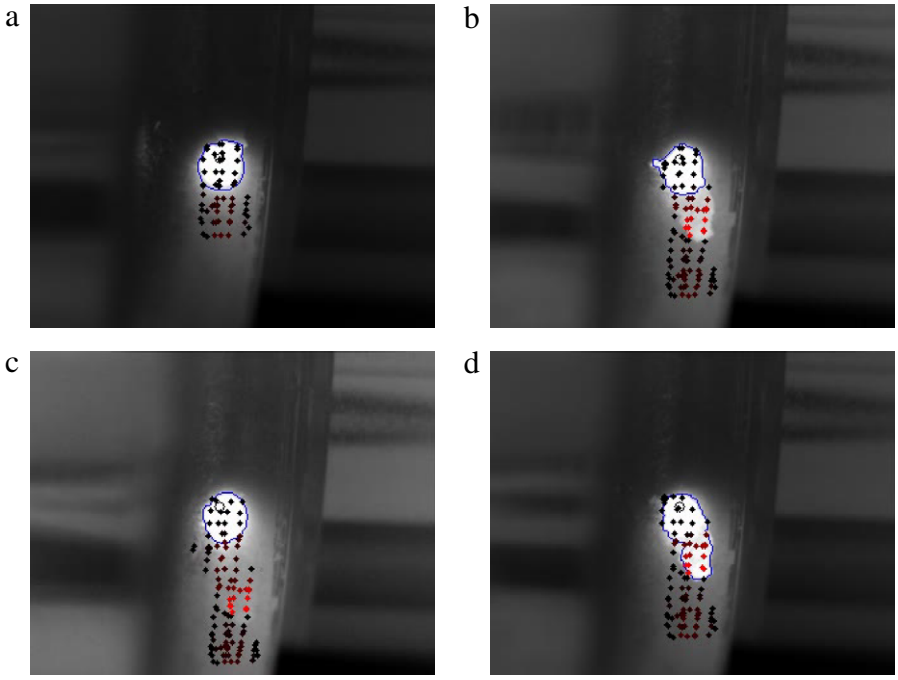

Fig. 9. Results of the ATP algorithm. When no thermal persistence is detected, the dots representing the past laser positions are drawn in a dark color (a). The color of the dots becomes lighter in (b), when some energy is trapped by a crack and its fade-out phase is slower than in normal conditions. The ATP tracks the regions where thermal persistence was found, even after the end of the persistence (c). In (d) the algorithm works even when the persistence is fused together with the main laser spot in a single blob. (For interpretation of the references to color in this figure legend, the reader is referred to the web version of this article.)

References

[1] T.S. Newman, A.K. Jain, A survey of automated visual inspection, Comput. Vis. Image Underst. 61 (2) (1995) 231–262.

[2] E.N. Malamas, E.G.M. Petrakis, M. Zervakis, L. Petit, J.-D. Legat, A survey on industrial vision systems, applications and tools, Image Vis. Comput. 21 (2) (2003) 171–188.

[3] M. Shirvaikar, Trends in automated visual inspection, J. Real-Time Image Process. 1 (1) (2006) 41–43.

[4] M.S. Millán, J. Escofet, Fabric inspection by near-infrared machine vision, Opt. Lett. 29 (13) (2004) 1440–1442.

[5] S. Ghidoni, M. Minella, L. Nanni, C. Ferrari, M. Moro, E. Pagello, E. Menegatti, Automatic crack detection in thermal images for metal parts. in: Proceedings of the International Conference on Heating by Electromagnetic Sources, May 2013.

[6] T. Ummenhofer, J. Medgenberg, On the use of infrared thermography for the analysis of fatigue damage processes in welded joints, Int. J. Fatigue 31 (1) (2009) 130–137.

[7] C. Neubauer, Intelligent x-ray inspection for quality control of solder joints, IEEE Trans. Compon. Packag. Manuf. Technol. Part C 20 (2) (1997) 111–120.

[8] S. Ghidoni, M. Minella, L. Nanni, C. Ferrari, M. Moro, E. Pagello, E. Menegatti, Automatic crack detection in thermal images for metal parts, in: Proceedings of the International Conference on Heating by Electromagnetic Sources 2013, May 2013, pp. 181–188.

[9] C. Eitzinger, S. Ghidoni, E. Menegatti, Thermobot: towards semi-autonomous, thermographic detection of cracks, in: Proceedings of the International Conference on Heating by Electromagnetic Sources 2013, May 2013, pp. 461–468.

[10] A. Gachagan, A. McNab, P. Reynolds, Analysis of ultrasonic wave propagation in metallic pipe structures using finite element modelling techniques, in: Ultrasonics Symposium, 2004 IEEE, vol. 2, IEEE, 2004, pp. 938–941.

[11] T. Theodoulidis, S. Panas, E. Kriezis, Eddy current detection of crack orientation using elliptical excitation, in: Science, Measurement and Technology, IEE Proceedings, vol. 141, IET, 1994, pp. 41–47.

[12] P. Xu, K. Shida, Eddy current sensor with a novel probe for crack position detection, in: 2008 IEEE International Conference on Industrial Technology, IEEE, 2008, pp. 1–6. IEEE.

[13] G. Tian, A. Sophian, D. Taylor, J. Rudlin, Multiple sensors on pulsed eddy-current detection for 3-D subsurface crack assessment, IEEE Sens. J. 5 (1) (2005) 90–96.

[14] J. Hwang, J. Kim, J. Lee, Magnetic images of surface crack on heated specimen using an area-type magnetic camera with high spatial resolution, in: Instrumentation and Measurement Technology Conference, 2009. I2MTC'09. IEEE, IEEE, 2009, pp. 1546–1551.

[15] A. Sophian, G. Tian, S. Zairi, Pulsed magnetic flux leakage techniques for crack detection and characterisation, Sensors Actuators A 125 (2) (2006) 186–191.

[16] T. Liu, Application of thermo-electric Joule heating for crack detection, in: 2010 2nd International Conference on Mechanical and Electronics Engineering, IEEE, vol. 1, IEEE, 2010, p. V1-103–V1-107.

[17] H. Shafeek, E. Gadelmawla, A. Abdel-Shafy, I. Elewa, Assessment of welding defects for gas pipeline radiographs using computer vision, NDT & E Int. 37 (4) (2004) 291–299.

[18] P. Prasanna, K. Dana, N. Gucunski, B. Basily, Computer-vision based crack detection and analysis, in: M.i Tomizuka, C. Yun, J. Lynch (Eds.), SPIE Smart Structures and Materials + Nondestructive Evaluation and Health Monitoring, International Society for Optics and Photonics, 2012, pp. 834542–834542-6.

[19] N. Turakhia, R. Shah, M. Joshi, Automatic crack detection in heritage site images for image inpainting, in: Proceedings of the Eighth Indian Conference on Computer Vision, Graphics and Image Processing, ACM, 2012, p. 68.

[20] M. Genest, D. Dudzinski, S. Bulmer, R. Kersey, Crack detection using induction thermography for thermomechanical fatigue tests, in: Review of Progress in Quantitative Nondestructive Evaluation: Volume 30A; Volume 30B, vol. 1335, AIP Publishing, 2011, pp. 1727–1734.

[21] D. Wagner, N. Ranc, C. Bathias, P. Paris, Fatigue crack initiation detection by an infrared thermography method, Fatigue Fract. Eng. Mater. Struct. 33 (1) (2010) 12–21.

[22] E. Kostson, B. Weekes, D. Almond, J. Wilson, G. Tian, Donald O. Thompson, Dale E. Chimenti, Crack detection using pulsed eddy current stimulated thermography, in: Review of Progress in Quantitative Nondestructive Evaluation: Volume 30A; Volume 30B, vol. 1335, AIP Publishing, 2011, pp. 415–422.

[23] X. Maldague, F. Galmiche, A. Ziadi, Advances in pulsed phase thermography, Infrared Phys. Technol. 43 (3–5) (2002) 175–181.

[24] T. Maffren, P. Juncar, F. Lepoutre, G. Deban, Crack detection in high-pressure turbine blades with flying spot active thermography in the SWIR range, in: Review of Progress in Quantitative Nondestructive Evaluation: Volume 31, vol. 1430, AIP Publishing, 2012, pp. 515–522.

[25] A. Besbes, N. Komodakis, G. Langs, N. Paragios, Shape priors and discrete MRFS for knowledge-based segmentation, in: IEEE Conference on Computer Vision and Pattern Recognition, 2009. CVPR 2009, IEEE, 2009, pp. 1295–1302.

[26] N. Paragios, M. Rousson, V. Ramesh, Knowledge-based registration & segmentation of the left ventricle: a level set approach, in: Proceedings. Sixth IEEE Workshop on Applications of Computer Vision, 2002, WACV 2002, IEEE, 2002, pp. 37–42.

[27] T. Möller, B. Trumbore, Fast, minimum storage ray-triangle intersection, J. Graph. Tools 2 (1) (1997) 21–28.

[28] P. Azad, T. Gockel, R. Dillmann, Computer Vision: Principles and Practice, Elector International Media BV 2008, 2008.

[29] G. Kylberg, M. Uppström, I. Sintorn, Virus texture analysis using local binary patterns and radial density profiles, in: Progress in Pattern Recognition, Image Analysis, Computer Vision, and Applications, Springer, 2011, pp. 573–580.

[30] J. Chen, S. Shan, C. He, G. Zhao, M. Pietikainen, X. Chen, W. Gao, Wld: A robust local image descriptor, IEEE Trans. Pattern Anal. Mach. Intell. 32 (9) (2010) 1705–1720.

[31] X. Qian, X.-S. Hua, P. Chen, L. Ke, Plbp: An effective local binary patterns texture descriptor with pyramid representation, Pattern Recognit. 44 (10) (2011) 2502–2515.

[32] T. Ojala, M. Pietikainen, T. Maenpaa, Multiresolution gray-scale and rotation invariant texture classification with local binary patterns, IEEE Trans. Pattern Anal. Mach. Intell. 24 (7) (2002) 971–987.
[33] Petter Strandmark, Johannes Ulén, Fredrik Kahl, Hep-2 staining pattern classification, in: 2012 21st International Conference on Pattern Recognition (ICPR), IEEE, 2012, pp. 33–36.
[34] N. Cristanini, J. Shawe-Taylor, An Introduction to Support Vector Machines and Other Kernel-based Learning Methods, first ed., Cambridge University Press, 2000.
[35] T. Fawcett, Roc graphs: Notes and practical considerations for researchers, Mach. Learn. 31 (2004) 1–38.

Stefano Ghidoni received the M.S. degree in Telecommunication Engineering and the Ph.D. degree in Information Technology from the University of Parma, Italy, in 2004 and 2008, respectively.

From 2004 to 2007 he worked in the field of artificial vision applied to the automotive field as a Ph.D. student of the Artificial Vision and Intelligent Systems Laboratory (VisLab), University of Parma, Italy. From 2008 to 2009, he worked in the artificial intelligence field at Henesis s.r.l., Parma, Italy, which is a spin-off company of the Scuola Superiore S. Anna di Pisa, Italy.

In March 2009 he joined the Intelligent Autonomous Systems Laboratory, University of Padova, Italy, as a Temporary Researcher, where he is currently working on intelligent video-surveillance systems, camera networks, and industrial visual inspection systems.

Mauro Antonello received his M.S. degree in Computer Science in 2010 from the University of Padova, Italy. Since 2011 he joined the Intelligent Autonomous Systems Lab (IAS-Lab) at the Department of Information Engineering, University of Padova, Italy, where he is a Ph.D. candidate. His research interests include models for object detection under multiple viewpoints, and stereo reconstruction of large outdoor environment for analysis of landslides.

Loris Nanni received the master degree cum laude from the University of Bologna, Italy, on June 2002. In December 2003 he started his Ph.D. studies at DEIS-University of Bologna and in April-2006 he received his Ph.D. degree in Computer Engineering. He was a Post Ph.D. fellow (from 2006 to 2011) at DEIS (department of Computer Engineering)—of University of Bologna. In December-2010 he won a position as Associate Researcher at the Department of Information Engineering—University of Padua (Padova). He is interested in: Bioinformatics; Biometric Systems; Multi-classifier systems; Image Database.

Emanuele Menegatti is Associate Professor of Computer Science in the School of Engineering of the University of Padova. He graduated in Physics (1998), he has a Master of Science in Artificial Intelligence at the University of Edinburgh (UK) (2000) and a Ph.D. in Computer Science (2003). In 2005, he became Assistant Professor. Since 2010, he is Associate Professor. His research interests are in the field of Robot Vision Perception. In particular, he has been working on omnidirectional vision systems for autonomous robots, on distributed vision systems, on 2D and 3D industrial robot vision, on automatic visual inspection, and on RGB-D vision algorithms for mobile robots.

In 2002, he was Visiting Researcher at University of Wakayama (JP), in 2004 he was at Georgia Institute of Technology (US) and at University of Osaka (JN).

He has been Principal Investigator of several research grants on robot vision. In particular, he was Local Investigator for two European Projects 3DComplete and FibreMap and he is European Coordinator of the European project Thermobot. He also served as Project Reviewer for the European Commission in FP7.

In 2005 he started IT + Robotics srl, a Spin-off company of the University of Padova, active in the field of intelligent industrial robotics.

He has served as a Program Committee member for several conferences and chaired several workshops. In 2014, he is General Chair of the 13th Intl. Conf. on Intelligent Autonomous Systems (IAS-13).

He was invited editor for three journal special issues and published more than 20 journal papers and more than 100 conference papers.